This manuscript has been submitted for publication in Hydrology and Earth System Sciences (HESS). HESS-discussion preprint and interactive comments are available https://doi.org/10.5194/hess-2020-643. Please note that, despite having undergone peer-review, the manuscript has yet to be formally accepted for publication. Subsequent versions of this manuscript may have slightly different content.

Relative humidity gradients as a key constraint on terrestrial water and energy fluxes

Yeonuk Kim[1], Monica Garcia[2], Laura Morillas[3], Ulrich Weber[4], T. Andrew Black[5], Mark S. Johnson[1,3,6]

[1]Institute for Resources, Environment and Sustainability, University of British Columbia, Vancouver, V6T1Z4, Canada.
[2]Department of Environmental Engineering, Technical University of Denmark, Lyngby, 2800, Denmark.
[3]Center for Sustainable Food Systems, University of British Columbia, Vancouver, V6T1Z4, Canada.
[4]Max Planck Institute for Biogeochemistry, Hans Knoell Strasse 10, 07745 Jena, Germany
[5]Faculty of Land and Food Systems, University of British Columbia, Vancouver, V6T1Z4, Canada.
[6]Department of Earth, Ocean and Atmospheric Sciences, University of British Columbia, Vancouver, V6T1Z4, Canada.

Correspondence to: Yeonuk Kim (yeonuk.kim.may@gmail.com)

Abstract. Earth's climate and water cycle are highly dependent on terrestrial evapotranspiration and the associated flux of latent heat. Despite its pivotal role, predictions of terrestrial evapotranspiration remain uncertain due to highly dynamic and spatially heterogeneous land surface dryness. Although it has been hypothesized for over 50 years that land dryness becomes embedded in atmospheric conditions, underlying physical mechanisms for this land-atmospheric coupling remain elusive. Here, we use a novel physically-based evaporation model to demonstrate that near-surface atmospheric relative humidity (*rh*) fundamentally coevolves with *rh* at the land surface. The new model expresses the latent heat flux as a combination of thermodynamic processes in the atmospheric surface layer. Our approach is similar to the Penman-Monteith equation but uses only routinely measured abiotic variables, avoiding the need to parameterize surface resistance. We applied our new model to 212 in-situ eddy covariance sites around the globe and to the FLUXCOM global-scale evaporation product. Vertical *rh* gradients were widely observed to be near zero on daily to yearly time scales for local as well as global scales, implying an emergent land-atmosphere equilibrium. This equilibrium allows for accurate evaporation estimates using only the atmospheric state and radiative energy, regardless of land surface conditions and vegetation controls. Our results also demonstrate that the latent heat portion of available energy (i.e., evaporative fraction) at local scales is mainly controlled by the vertical *rh* gradient. By demonstrating how land surface conditions become encoded in the atmospheric state, this study will improve our fundamental understanding of Earth's climate and the terrestrial water cycle.

1 Introduction

Latent heat flux (*LE*) associated with plant transpiration and evaporation from soil and intercepted water (i.e., evapotranspiration, ET) links the water cycle with the terrestrial energy budget. More than half of the incoming radiation energy at the land surface is consumed as *LE*, making ET the second largest flux in the terrestrial water balance after precipitation (Oki and Kanae, 2006). Also, *LE* is a controlling factor for near-surface climatic conditions (Ma et al., 2018;Byrne and O'Gorman, 2016). However, *LE* predictions remain highly uncertain due to the high spatial and temporal variability in land surface dryness, and the difficulty of generalizing the physiological control of ET by stomata. While most research has been devoted to developing and improving rate-limiting parameters constraining *LE* (e.g., García et al., 2013;Martens et al., 2017), exploring the governing physics of *LE* has received less attention following earlier pioneering work (Penman, 1948;Bouchet, 1963;Monteith, 1965;Priestley and Taylor, 1972).

Climatic conditions over the land surface are getting not only warmer but also drier in recent decades (i.e., decrease in relative humidity) (Sherwood and Fu, 2014;Willett et al., 2014;Byrne and O'Gorman, 2018), but land-atmosphere feedback processes shaping the near-surface atmospheric state are still not well understood. In the early 1960's, Bouchet (1963) hypothesized that land surface dryness is coupled to the atmospheric state through *LE*, with the Bouchet hypothesis now widely accepted (Ramírez et al., 2005;Fisher et al., 2008;Mallick et al., 2014). However, the underlying physical mechanisms for this land-atmospheric coupling still remain elusive (McNaughton and Spriggs, 1989). Recently, McColl et al. (2019) introduced a novel theoretical perspective on land-atmosphere coupling which is referred to as "Surface Flux Equilibrium (SFE)". They hypothesized that the surface moistening and heating terms are balanced in the *rh* budget of an idealized atmospheric boundary layer at daily to monthly timescale. Under the SFE conditions, *LE* can be determined using only the atmospheric state and radiative energy. Although this method performed well compared to actual *LE* observations for inland continental sites (McColl and Rigden, 2020), a further investigation is needed to understand how dynamics of turbulent heat fluxes in the atmospheric surface layer at sub-daily time scale evolve to the SFE state.

A traditional way to understand the governing physics of the atmospheric surface layer processes is to partition *LE* into diabatic and adiabatic processes using the Penman-Monteith (PM) equation (Monteith, 1965), as proposed by Monteith (1981). The PM equation combines the energy balance equation with mass-transfer theory for water vapour and sensible heat, resulting in diabatic (radiative energy-related) and adiabatic (vapour pressure deficit-related) processes for a parcel of air in contact with a saturated surface (Monteith, 1981).

$$LE = \underbrace{\frac{S}{S+\gamma\left(\frac{r_a+r_s}{r_a}\right)} \cdot Q}_{Diabatic\ process} + \underbrace{\frac{\rho c_p}{S+\gamma\left(\frac{r_a+r_s}{r_a}\right)} \cdot \frac{e^*(T_a)-e_a}{r_a}}_{Adiabatic\ process} \quad (1)$$

where S is the linearized slope of saturation vapour pressure versus temperature (hPa K^{-1}), γ is the psychrometric constant (hPa K^{-1}), ρ is the air density (kg m^{-3}), c_p is the specific heat capacity of air at constant pressure (MJ kg^{-1} K^{-1}), and Q is available radiative energy (i.e., the difference between net radiation (R_n) and soil heat flux (G) and expressed in units of W m^{-2}). $e^*(T_a)$ is the saturation vapour pressure (hPa) corresponding to the air temperature (T_a) measured at a reference height (typically 2 m

or eddy flux measurement height), and e_a is vapour pressure (hPa) at the reference height. $e^*(T_a)$- e_a is known as atmospheric vapour pressure deficit (VPD, expressed in units of hPa). r_a is aerodynamic resistance to heat and water vapour transfer (s m^{-1}), and r_s is surface resistance to water vapour transfer (s m^{-1}) representing drying soil and/or plant stomatal closure.

In principle, high VPD at the reference height increases the adiabatic term in Eq. (1) (Monteith and Unsworth, 2013). Yet, this "high VPD leads to high *LE*" interpretation cannot be generalized because r_s increases with VPD due to stomatal closure by vegetation under high VPD conditions (Tan et al., 1978;Novick et al., 2016;Massmann et al., 2019). While the PM equation is useful to explore biological control of *LE* through r_s (Jarvis and McNaughton, 1986), physical mechanisms corresponding to each term in Eq. (1) are less intuitive due to the sensitivity of r_s to VPD.

Is there a way to mathematically express the physical mechanisms of *LE* without requiring r_s? Helpfully, Monteith (1981) provided another form of the *LE* model for the case when the surface does not reach saturation (i.e., the relative humidity (*rh*) of the surface is less than unity), and for which r_s is not required. Here, we further find that there are two mathematical expressions of *LE* which are capable of accounting for the vertical gradients in *rh*. The following equations allow us to capture the thermodynamic process governing turbulent heat exchange between the land surface and the atmosphere, including conditions for which the land surface is unsaturated (derivation in Appendix A).

$$LE = \underbrace{\frac{rh_s S}{rh_s S+\gamma}\cdot Q}_{Diabatic\ process:\ LE_Q} + \underbrace{\frac{\rho c_p e^*(T_a)}{rh_s S+\gamma}\cdot\frac{rh_s - rh_a}{r_a}}_{Adiabatic\ process:\ LE_G} = LE_Q + LE_G \quad (2)$$

$$LE = \underbrace{\frac{rh_a S}{rh_a S+\gamma}\cdot Q}_{Diabatic\ process:\ LE_{Q'}} + \underbrace{\frac{\rho c_p e^*(T_s)}{rh_a S+\gamma}\cdot\frac{rh_s - rh_a}{r_a}}_{Adiabatic\ process:\ LE_{G'}} = LE_Q{}' + LE_G{}' \quad (3)$$

where rh_s and rh_a are *rh* at the land surface and the reference height, respectively. Equations (2) and (3) include rh_s to compensate for eliminating r_s from the original PM equation. Since the adiabatic process in Eqs. (2) and (3) are controlled by the vertical difference of *rh*, we refer to Eqs. (2) and (3) as the proposed PM_{rh} model (Penman-Monteith equation expressed using *rh*) to distinguish it from the original PM model. The two equations represent different thermodynamic paths which will be discussed in the next section. Arguably, applying PM_{rh} can provide new insights into the fundamental mechanisms of *LE*, particularly when it is decomposed into its energy driven diabatic component (LE_Q or LE_Q') and its adiabatic component (LE_G or LE_G') that is driven by the gradient in *rh*.

In this paper, we first present the theory of our PM_{rh} model, and apply it empirically to eddy-covariance observation sites. Also, the proportion of net available energy consumed in evapotranspiration, known as the evaporative fraction ($EF = \frac{LE}{Q}$) is decomposed into $\frac{LE_Q}{Q}$ and $\frac{LE_G}{Q}$. Finally, we apply the decomposition approach to a global *LE* dataset to understand how LE_Q and LE_G vary spatiotemporally in different regions of the world, and discuss how these patterns can help to understand land-atmosphere interactions and potential responses under future climatic conditions.

2. Theory

2.1. Generalized Penman equation

Before discussing PM_{rh} in-depth, we revisit the Penman equation (Penman, 1948) to help with the physical reasoning behind our proposed framework. The widely recognized form of the Penman equation, which was developed as an *LE* model for a saturated surface, is as follows:

$$LE = \underbrace{\frac{S}{S+\gamma} \cdot Q}_{Diabatic\ process} + \underbrace{\frac{\rho c_p [e^*(T_a) - e_a]}{[S+\gamma] r_a}}_{Adiabatic\ process} \quad (4)$$

We rearrange this formulation to derive Eq. (5) by factoring out $e^*(T_a)$ and introducing $rh_a = \frac{e_a}{e^*(T_a)}$ into the second term.

$$LE = \underbrace{\frac{S}{S+\gamma} \cdot Q}_{Diabatic\ process} + \underbrace{\frac{\rho c_p e^*(T_a)}{S+\gamma} \cdot \frac{1 - rh_a}{r_a}}_{Adiabatic\ process} \quad (5)$$

Equations (4) and (5) are mathematically equivalent, but their interpretations are quite different. In Eq. (4), the adiabatic process is controlled by VPD at the reference height. However, in Eq. (5), the adiabatic process acts over the vertical *rh* gradient, i.e. the difference in *rh* from the surface (rh_s) to the reference height (rh_a). Since the Penman equation is a model for saturated surfaces, $1 - rh_a$ in Eq. (5) indicates the difference in *rh* over the vertical distance between the ground surface and the reference height. Arguably, Eq. (5) is more thermodynamically sound compared to Eq. (4) since *rh* is an ideal-gas approximation to the water activity (Lovell-Smith et al., 2015) which represents the chemical potential of water (μ_w) (Monteith and Unsworth, 2013;Kleidon and Schymanski, 2008). When the vertical gradient of *rh* dissipates, the land surface and the atmosphere are in thermodynamic equilibrium (Kleidon et al., 2009). Therefore, taking Eq. (5) instead of Eq. (4) allows us to view the adiabatic process of the Penman model as an equilibration process driving land-atmosphere equilibrium by bringing the surface μ_w to that of the atmosphere.

As with our interpretation of the Penman model, we can view Eq. (2), as a generalized form of the Penman model. Here, the LE_G ($= \frac{\rho c_p e^*(T_a)}{rh_s S+\gamma} \frac{rh_s - rh_a}{r_a}$) term of Eq. (2) is an equilibration process between the land and the atmosphere when the land surface is not saturated. It is worth noting that LE_G can be negative when rh_s is less than rh_a. Thus, the LE_G term acts to reduce the vertical *rh* gradient. This physical interpretation is consistent with recent findings that the variance of the *rh* gradient tends to be minimized over the course of the day, implying that the difference between rh_s and rh_a is reduced (Salvucci and Gentine, 2013;Rigden and Salvucci, 2015). The diabatic LE_Q ($= \frac{rh_s S}{rh_s S+\gamma} Q$) term can be understood as equilibrium *LE* for an unsaturated surface, which we discuss later in section 2.3.

2.2. Thermodynamic paths

How can we interpret the two formulas of PM_{rh} in Eqs. (2) and (3)? To explain the two forms, the psychrometric relationship is applied to a parcel of air near an unsaturated land surface that is under constant pressure and steadily receiving

radiation energy (Monteith, 1981). The initial thermodynamic state of the air parcel can be represented by its temperature and water vapour pressure such as point A in Fig. 1. The initial state is changed by two processes as follows: (1) equilibrating between the land surface (rh_s) and the air parcel (rh_a), and (2) increasing enthalpy forced by the incoming energy.

In the equilibrating process, the air parcel is adiabatically cooled (or heated when $rh_s < rh_a$), while the enthalpy of the parcel is not changed. Therefore, the increase (decrease) in latent heat content in the parcel is exactly balanced by a decrease (increase) in sensible heat ($A \rightarrow B$ in Fig. 1: trajectory along constant enthalpy line). This process is equivalent to the LE_G term in Eq. (2). Now, the air parcel is in thermodynamic equilibrium with the land surface (point B in Fig. 1). Then, the air parcel receives energy while the equilibrium is sustained (i.e., rh_s is steady), which increases both the temperature and absolute water vapour content of the air parcel ($B \rightarrow C$ in Fig. 1). This process can be expressed as LE_Q of Eq. (2). Consequently, the thermodynamic state of the air parcel approaches point C in Fig. 1.

However, we should recognize that temperature and vapour pressure are "state" variables meaning that they do not depend on the thermodynamic path by which the system arrived at its final state (Iribarne and Godson, 2012). In the above example, we conceptually followed the adiabatic process first and then the diabatic process (Path 1 in Fig. 1), but one can imagine the opposite order. If we choose Path 2 in Fig. 1, the diabatic process comes first, and thus rh_a instead of rh_s is preserved while enthalpy increases (i.e., LE_Q'), and the adiabatic process is followed at temperature of T_S (i.e., LE_G'). Path 2 is described by Eq. (3).

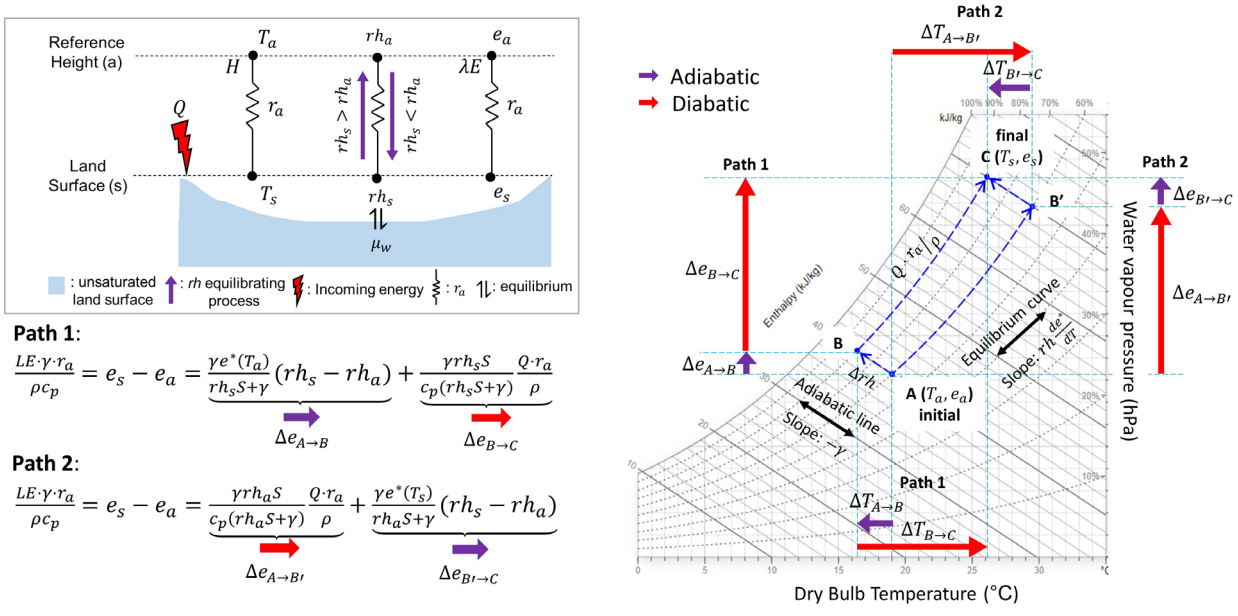

Figure 1: Schematic conceptualization of the PM_{rh} model and psychrometric relationship of PM_{rh}. The example psychrometric chart is modified from drajmarsh.bitbucket.io/psychro-chart2d.html. Path 1 represents Eq. (2) divided by $\frac{\rho c_p}{\gamma r_a}$ while Path 2 represents Eq. (3) divided by $\frac{\rho c_p}{\gamma r_a}$. Here, the enthalpy change of the air parcel is defined as $\frac{Q \cdot r_a}{\rho}$ (kJ kg^{-1}).

Therefore, one can interpret the two forms of PM_{rh} in Eqs. (2) and (3) as two thermodynamic paths where the diabatic and adiabatic processes occur simultaneously. It should be noted that the diabatic and adiabatic processes in PM_{rh} are "path" functions and thus they vary by path. For instance, LE_Q is slightly higher than LE_Q' when $rh_s > rh_a$.

2.3. Equilibrium *LE* for an unsaturated surface

Another distinct characteristic of the PM_{rh} model is the way it defines equilibrium at the land-atmosphere interface. Unlike many previous studies which focused on the VPD budget (McNaughton and Jarvis, 1983;Priestley and Taylor, 1972;Raupach, 2001), land-atmosphere equilibrium is achieved in the PM_{rh} model when the vertical *rh* gradient (i.e., the μ_w gradient) dissipates. That is, if $rh_s \approx rh_a$, then it follows that LE_G (or LE_G') is zero and thus *LE* becomes

$$LE \approx \frac{rh_a S}{rh_a S+\gamma} Q \quad (6)$$

We note that Equation (6) is identical to the SFE theory recently introduced by McColl et al. (2019). They hypothesized that in many continental regions, the near surface atmosphere is in state of equilibrium, where the surface moistening and surface heating terms are balanced in the *rh* budget, especially at longer time scales. Equation (6) successfully predicted observed *LE* at daily and multiday time scales for inland regions (McColl and Rigden, 2020), which implies the vertical *rh* gradient tends to zero. This is logical in that LE_G itself operates to diminish the vertical *rh* gradient.

When both land surface and atmosphere are saturated (i.e., $rh_s \approx rh_a \approx 1$), equation (6) becomes classical equilibrium *LE* (i.e., $LE \approx \frac{S}{S+\gamma} Q$). This is consistent with a classical definition of equilibrium *LE* that defines equilibrium *LE* as evaporation from a saturated surface into saturated air (Eichinger et al., 1996;Raupach, 2001;McColl, 2020). Therefore, we can regard Eq. (6) as a generalized equilibrium *LE* for an unsaturated surface.

3. Materials and Methods

In the following sections, we present a novel physical decomposition of *LE* from PM_{rh} into LE_Q and LE_G components to aid in understanding the governing physics of *LE*. We conducted a detailed diagnostic analysis of the PM_{rh} model using the multi-year record of an eddy covariance (EC) flux observation site located in a wet-dry tropical climate. We also applied the PM_{rh} model to the 212 EC sites represented in the FLUXNET2015 dataset (Pastorello et al., 2020), and to the FLUXCOM global *LE* product (Jung et al., 2019). We describe the local and global datasets and analysis methods here before presenting the results.

3.1. In-situ EC flux observation

In-situ half-hourly EC observations used in this study were made from 2015 to 2018 on a ratoon sugarcane farm in the province of Guanacaste, Costa Rica (10°25′07.60″N; 85°28′22.22″W). The site has a wet-dry tropical climate with a dry season from December to March and a median monthly air temperature ranging from 27 °C to 30 °C. The study site experienced a

significant drought in 2015 (Hund et al., 2018;Morillas et al., 2019). The site was irrigated occasionally during dry seasons via furrow irrigation events, except for 2016 when there was no irrigation due to crop replanting. Due to the ratooning practice (i.e., sugarcane cutting each year followed by resprouting without replanting, detailed explanation in the Supplement), the sugarcane growing seasons varied by year, which provided an opportunity to explore distinct and varied combinations of land surface vs. atmospheric aridity conditions.

The measured *LE* and sensible heat flux (*H*) were quality controlled following Morillas et al. (2019) (details in the Supplement). For the study period, the surface energy balance closure (i.e., $\frac{LE+H}{R_n-G}$) of 30 min data was 86 %, which is typical of high-quality eddy-covariance data sets (Wilson et al., 2002). When canopy height was less than 1 m, the surface energy balance was almost closed (97%), whereas the closure was 83 % when canopy height was higher than 1 m. Considering a possible significant role of unmeasured canopy and soil heat storages (Leuning et al., 2012;Eshonkulov et al., 2019) and the homogenous landscape of the study site (Foken, 2008;Stoy et al., 2013), we did not force the energy closure. Therefore, we defined Q as the sum of *LE* and *H* instead of $R_n - G$. In doing so, we in effect attribute the cause of the surface energy imbalance to unmeasured heat storage terms following Moon et al. (2020).

In order to decompose *LE* into LE_Q and LE_G, we first estimated half-hourly aerodynamic resistance (r_a) by considering aerodynamic resistance to momentum transfer and the additional boundary layer resistance for heat and mass transfer (or excess resistance) (Thom, 1972;Knauer et al., 2018).

$$r_a = \frac{ln[\frac{z_r-d}{z_{0m}}]-\psi_h}{ku_*} + 6.2u_*^{-0.67} \quad (7)$$

The first term on the right-hand side of Eq. (7) is the aerodynamic component and the second term is the boundary layer component. Here, u_* is friction velocity, k is the von Kármán constant (0.41), d is the zero-plane displacement height ($d = 0.7z_h$), z_{0m} is the roughness length for momentum ($z_{0m} = 0.1z_h$), ψ_h is the integrated form of the stability correction function. z_h is canopy height based on manual measurements taken during regular maintenance visits. r_a was estimated using bigleaf R package (Knauer et al., 2018).

By rearranging Eq. (2), rh_s can be calculated using

$$rh_s = \frac{\gamma LE r_a/\rho c_p + e_a}{SH r_a/\rho c_p + e^*(T_a)} \quad (8)$$

Negative *H* and inaccurate r_a modelling sometimes yielded negative rh_s or values greater than one, especially at nighttime. In these cases, rh_s was assigned the value of one following the approach described in the bigleaf R package (Knauer et al., 2018). We then estimated LE_Q and LE_G from Eq. (2).

In order to explore the time scale of the covariances for $LE \sim LE_Q$ and $LE \sim LE_G$ in the frequency domain, we applied wavelet coherence analysis using WaveletComp R package (Roesch and Schmidbauer, 2014). The package is designed to apply the continuous wavelet transform using Morlet wavelet, which is a popular approach to analyze hydrological and micrometeorological datasets (Hatala et al., 2012;Johnson et al., 2013). A total time series of half-hourly decomposed *LE* for the 4-year measurement period was used to estimate localized coherence and phase angle. The wavelet coherence can be

interpreted as the local correlation between two variables in the frequency-time domain (where red indicates high correlation). A 0° phase angle (arrow pointing right) indicates periods of positive correlation while a 180° phase angle (arrow pointing left) indicates periods of negative correlation.

3.2. FLUXNET2015

The daily scale FLUXNET2015 dataset, which includes 212 empirical eddy-covariance flux tower sites around globe (Pastorello et al., 2020), was used in this study. The turbulent heat fluxes, net radiation, soil heat flux, air temperature, relative humidity, wind speed, friction velocity, and barometric pressure were obtained from the dataset. For this analysis, we only included daily data for periods for which the quality control flag indicated more than 80 % half-hourly data were present (i.e., measured data in general, or good quality gap-filled data in cases of partially missing data).

In order to decompose daily *LE* into LE_Q and LE_G, we estimated daily aerodynamic resistance (r_a) by Eq. (9) instead of Eq. (7) since canopy and measurement heights are unknown (Thom, 1972;Knauer et al., 2018).

$$r_a = \frac{u_*^2}{u(z_r)} + 6.2u_*^{-0.67} \quad (9)$$

where, $u(z_r)$ is reference height wind speed. r_a was estimated using the bigleaf R package (Knauer et al., 2018) and rh_s was calculated from Eq. (8).

LE_Q and LE_Q' were calculated using rh_a and rh_s following Eqs. (2) and (3), and then LE_G and LE_G' were calculated by subtracting LE_Q and LE_Q' from *LE*. To calculate LE_Q and LE_Q', we define Q as $LE + H$, but it should be noted that this approach can include systematic uncertainty since the sum of *LE* and *H* measured by eddy covariance is typically lower than $R_n - G$ (i.e., conditions referred to as the energy balance closure problem (Wilson et al., 2002)). To investigate the effect of a lack of energy balance closure on resulting *LE* terms, we provide Fig. S1 that was generated by 1) defining Q as $R_n - G$, and 2) correcting *LE* and *H* based on the assumption that the Bowen ratio ($B = H/LE$) is correct (Pastorello et al., 2020).

3.3. FLUXCOM

The FLUXCOM dataset (Jung et al., 2019) is a global-scale machine learning ensemble product which upscales FLUXNET observations (Baldocchi et al., 2001) using Moderate Resolution Imaging Spectroradiometer (MODIS) satellite data and reanalysis meteorological data. In this study we used the monthly *LE* FLUXCOM dataset (0.5° resolution) modelled using MODIS and ECMWF ERA5 reanalysis data (Hersbach et al., 2020).

We obtained Q and *LE* from the FLUXCOM output, and air temperature and dewpoint temperature were retrieved from ERA5 monthly averaged data (2 m height). *rh*, *S*, and γ were calculated from ERA5 data, and then LE_Q' was calculated. LE_G' was then estimated by subtracting LE_Q' from *LE*.

4. Results

4.1. Decomposition analysis of in-situ EC flux observation

Application results of the PM_{rh} model to the observed *LE* at an irrigated sugarcane farm in Costa Rica are depicted in Fig. 2. The decomposition analysis of observed *LE* shows that while LE_Q is the major component of *LE*, LE_G variability plays a non-negligible role in seasonal and interannual behaviour of *LE.* In terms of absolute magnitude, LE_Q term can closely approximate *LE,* and LE_G only represents 15% of total evaporation. Also, positive coherence between *LE* and LE_Q was strong over the entire period of observation, particularly at diurnal to multiday time scales (0.5~32 days), implying variability of *LE* is largely determined by LE_Q variability (i.e., red colored regions in Fig. 2 (c)).

Nevertheless, *LE* and LE_G also had a strong positive correlation in longer time scales (32~365 days) (i.e., red colored regions in Fig. 2 (d)). When the land surface is dry after harvests or no dry season irrigation, a negative correlation between *LE* and LE_G at diurnal time scale was observed. Also, we found that EF variability is mostly determined by LE_G variability since the diurnal and seasonal signal of *Q* is removed from *LE* in EF. Interestingly, the annual mean LE_G was the highest in 2015, a drought year in which rh_a was generally lower than for the other years, while the annual mean LE_G was close to zero in 2016 when there was no application of dry season irrigation due to crop replanting.

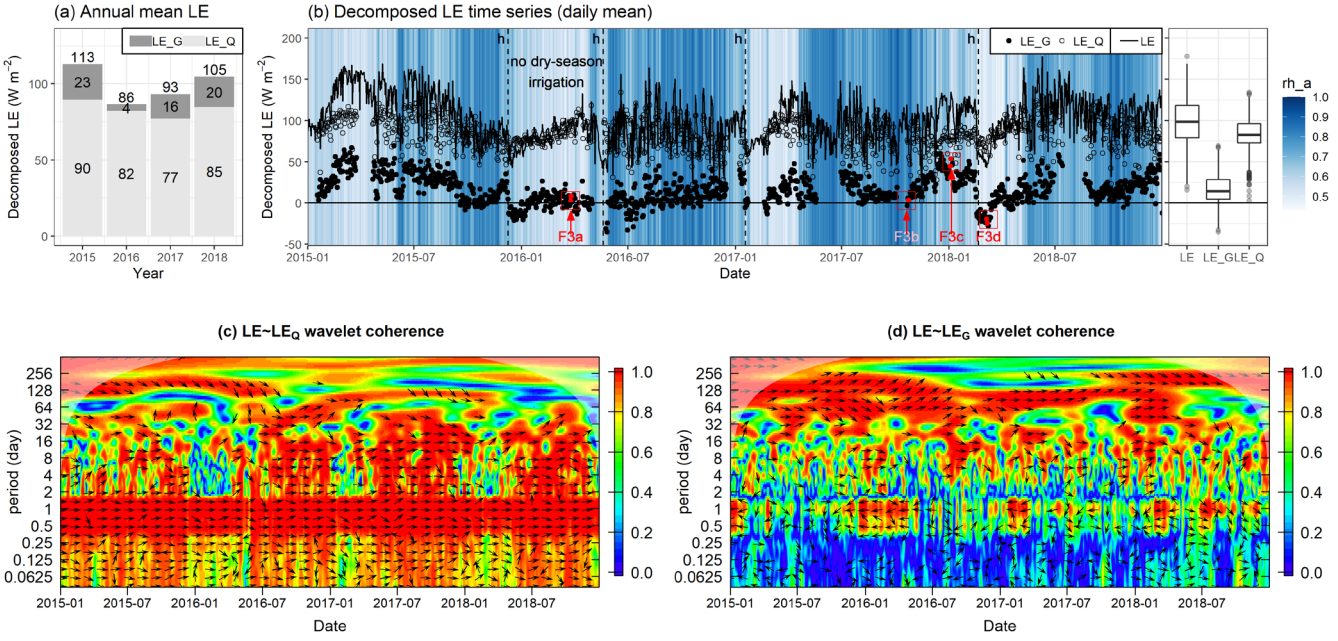

Figure 2: Time series of *LE*, LE_Q, and LE_G for the sugarcane EC tower site in Costa Rica. Panel (a) is mean annual *LE* and its components and (b) is a time series of daily mean values with a background color of rh_a. Dashed lines with "h" in panel (b) indicate sugarcane harvest. Panels (c) and (d) are wavelet coherence of *LE* with LE_Q and *LE* with LE_G. Red and blue colors indicate high and low correlation, respectively. Arrows (pointing right: in-phase; left: antiphase) only appear when the coherence is significant ($p<0.01$).

To explore the diurnal behaviour of decomposed *LE*, we selected different surficial and atmospheric conditions when LE_G was zero, positive, or negative in Fig. 3. In the 2016 dry season, LE_G was close to zero as a daily average value, as a result of negative daytime and positive nighttime LE_G values due to dry air and dry soil conditions (no irrigation) and an undeveloped vegetation canopy (Fig. 3 (a)). Daily LE_G was also close to zero during wet season conditions (e.g., Fig. 3 (b)). In this case, LE_G was near zero during both daytime and nighttime periods due to near saturated atmospheric and land surface conditions. These two cases show that "dry land-dry air" or "wet land-wet air" conditions can each lead to daily scale land-atmosphere equilibrium, although the diurnal pattern of LE_G is starkly different for dry land-dry air vs. wet land-wet air conditions.

Meanwhile, when rh_a was low and the canopy was well-developed, LE_G was found to be positive during both daytime and nighttime periods (Fig. 3 (c)). On the other hand, during post-harvest conditions when vegetative canopy cover was minimal and air and soil moisture levels were low, daily LE_G was found to be negative as a result of negative daytime and positive nighttime LE_G (Fig. 3 (d)). Regarding the overall diurnal pattern, LE_G generally declined during the morning and increased in the afternoon, which is consistent with the well-known diurnal pattern of EF (Gentine et al., 2011;Gentine et al., 2007) (Fig. 3 (e)).

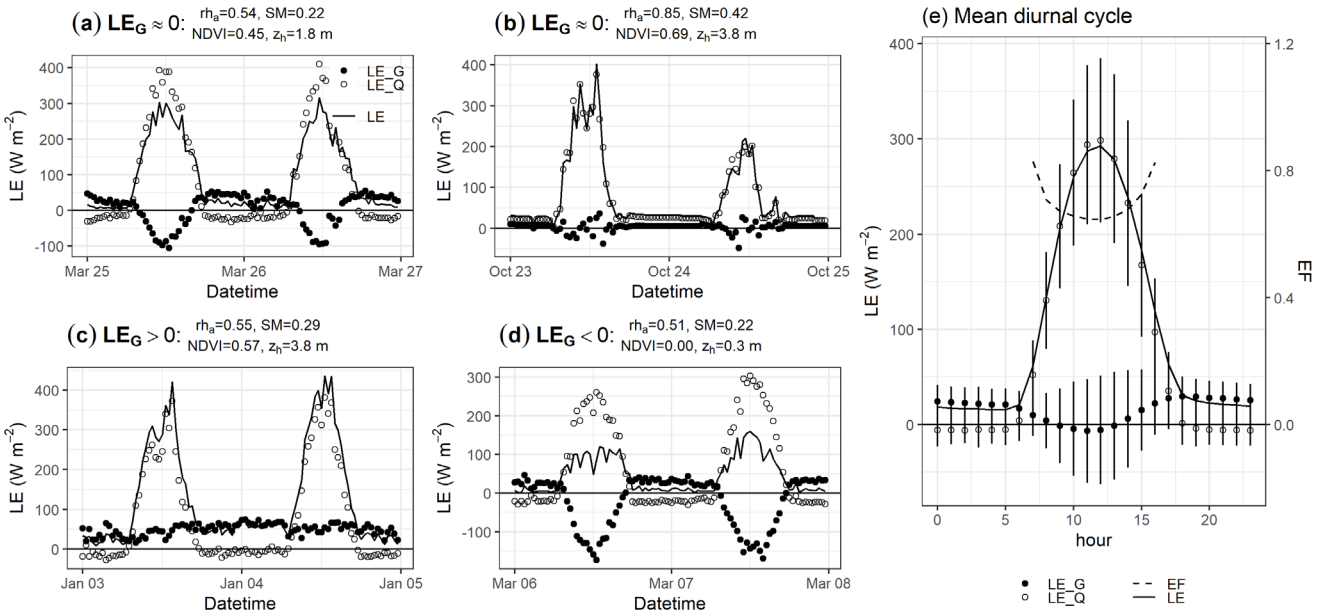

Figure 3: Half-hourly time series indicated in Figure 2 (b). Here, rh_a is mean atmospheric relative humidity, SM is volumetric soil water content, NDVI is normalized difference vegetation index, and z_h is canopy height. Panel (e) presents the long-term mean diurnal cycle of decomposed *LE* (dots) and EF (dashed line).

4.2. Decomposition analysis of FLUXNET2015 dataset

One of the interesting findings from the decomposition analysis of FLUXNET2015 dataset was that differences between LE_Q (Eq. (2)) and LE_Q' (Eq. (3)), as well as differences between LE_G and LE_G', are marginal at a daily time scale (Fig. 4 (a1) and (a2)). This result implies that although the diabatic and adiabatic processes expressed by Eqs. (2) and (3) are different in magnitude (see section 2.2), their difference is practically negligible. This is an important point since LE_Q' can be determined simply and directly using by reference height meteorological measurements, while LE_Q is required to know rh_s.

Another important finding of the decomposition analysis is the global-scale land-atmosphere equilibrium. Our analysis in Fig. 4 indicates that the mean value of daily LE_G of all FLUXNET2015 sites is close to zero, implying the global mean *rh* gradient is near zero at a daily time scale. Importantly, *LE* is primarily determined by LE_Q ($R^2 = 0.65$) instead of LE_G ($R^2 = 0.18$). Nevertheless, FLUXNET2015 data also suggests that LE_G is the main driver of local-scale variability of EF at the daily time scale (Fig. 4 (c1) and (c2)). It should be noted that Fig. 4 and Fig. S1 (energy balance corrected version) are almost identical, implying that the lack of surface energy balance closure for EC observations does not significantly impact our analyses and interpretations.

4.3. Decomposition analysis of FLUXCOM dataset

We then applied the PM_{rh} model to the FLUXCOM dataset, a benchmark global *LE* data product (Jung et al., 2019). As shown in Fig. 5 (a) and (c), the spatial patterns of the annual mean *LE* and LE_Q' were similar. The monthly time series of global *LE* and its two components in Fig. 5 (e1) show that LE_G' is consistently close to zero and that spatial variability of *LE* is mostly determined by LE_Q' ($R^2 = 0.85$) rather than by LE_G' ($R^2 = 0.18$) (Fig 5. (f1) and (f2)). This result is consistent with Eq. (6) and the SFE theory. In other words, the land surface is generally under thermodynamic equilibrium with the atmosphere at the global-annual scale (i.e., $rh_s \approx rh_a$).

However, while mean annual LE_G' was close to zero in broad areas (particularly in high latitude regions), it was distinctly positive or negative at the annual scale for many regions (Fig. 5 (d)). In humid tropical regions like the Amazon basin where moisture convergence is large, LE_G' was generally positive, whereas arid regions such as Australia were characterized by negative LE_G' (Fig. 5 (e3) and (e4)). Here, positive LE_G' (i.e., $rh_s > rh_a$) indicates the land surface is wetter than the near-surface atmosphere while negative LE_G' (i.e., $rh_s < rh_a$) implies a drier land surface than the atmosphere. The spatial pattern of LE_G' is similar to the spatial pattern of EF (Fig. 5 (b)). The finding that that the spatial variation of EF is primarily controlled by LE_G' instead of LE_Q' was supported by correlation analyses ($R^2 = 0.60$ for EF~LE_G' and $R^2 = 0.28$ for EF~LE_Q'; Fig. 5 (f3) and (f4)).

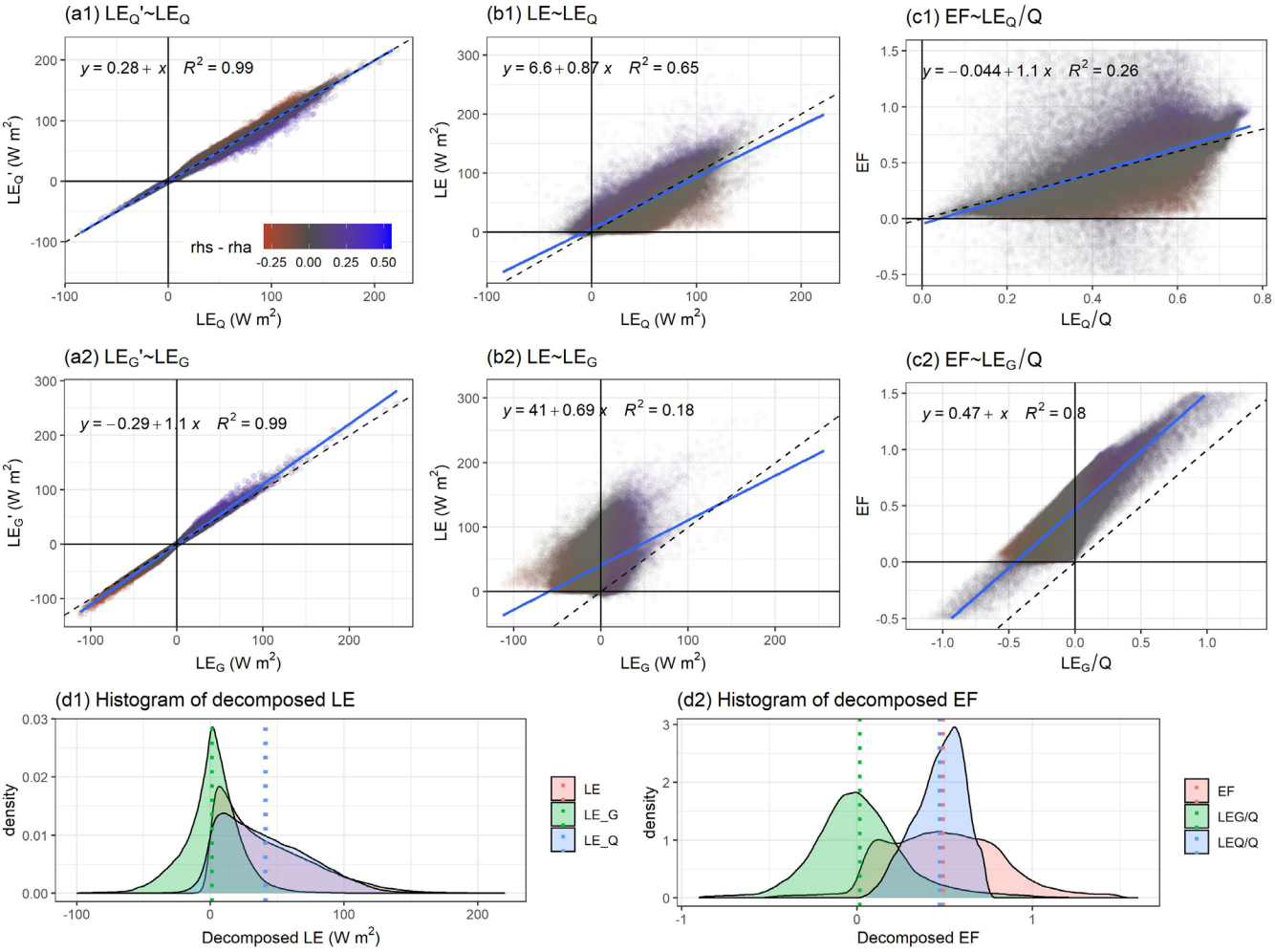

Figure 4: FLUXNET2015 daily scale decomposed *LE* for 212 sites and 1532 site-years. Panels (a1) and (a2) are linear regressions of LE_Q' on LE_Q and LE_G' on LE_G. Panels (b1) and (b2) are linear regressions of *LE* on LE_Q and *LE* on LE_G. Panels (c1) and (c2) are linear regressions of EF on LE_Q/Q and EF on LE_G/Q. In these panels, daily EF data within a range from -1 to 1.5 are only shown. Here, dashed lines are one-to-one lines, blue lines are regression lines, and color represents $rh_s - rh_a$. Panel (d1) and (d2) are histograms of decomposed *LE* and EF with mean values (dotted lines). To correct for lack of energy balance closure, *Q* was set equal to *LE*+*H* in all calculations.

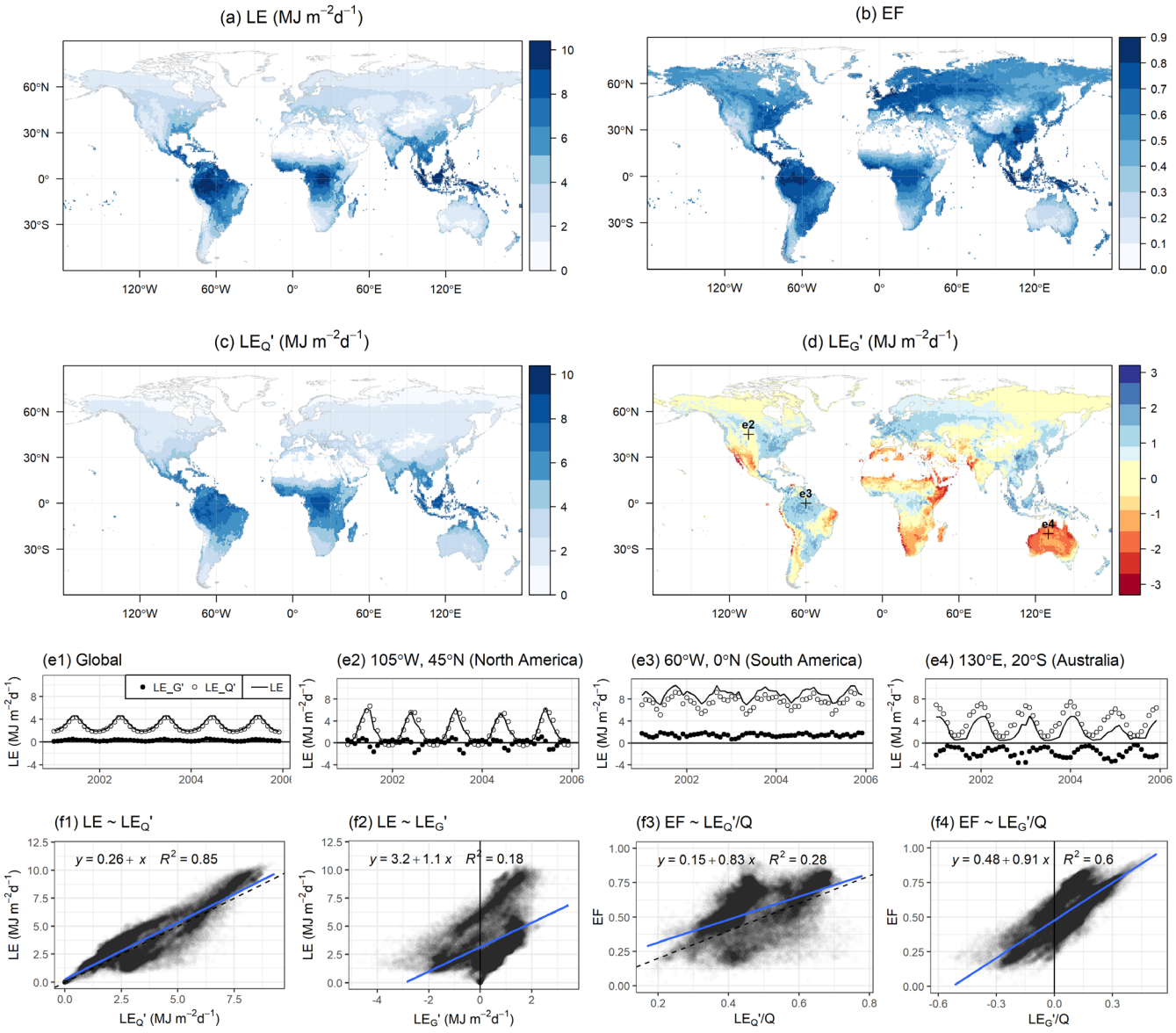

305 **Figure 5: Mean annual *LE*, EF, *LE*$_Q$', and *LE*$_G$' from 2001 to 2005 (panels (a), (b), (c), and (d), respectively). Panel (e1) is a time series of monthly global average *LE* and the two components, *LE*$_G$' and *LE*$_Q$'. Panels (e2), (e3), and (e4) are time series at specific locations highlighted in panel (d). Panels (f1), (f2), (f3), and (f4) are spatial linear regressions of *LE* on *LE*$_Q$', *LE* on *LE*$_G$', EF on *LE*$_Q$'/*Q*, and EF on *LE*$_G$'/*Q*, respectively.**

5. Discussion

Salvucci and Gentine (2013) found that the variance of the *rh* gradient tends to be minimized over the course of the day. Based on this empirical finding, they developed an approach to predict *LE* only using standard meteorological measurements, and this approach accurately predicted actual *LE* (Rigden and Salvucci, 2015, 2017). Our PM_{rh} model provides theoretical support for their approach in that LE_G acts to reduce the *rh* gradient. Indeed, the U-shape diurnal cycles of LE_G in Fig. 3 (positive nighttime and negative daytime) show the direction and the magnitude of the equilibration process of *rh* gradient at a sub-daily scale resulting in a small gradient of *rh* on daily average.

Over the course of the day, rh_a coevolves with rh_s through the equilibration process, and thus the land surface moisture status is linked to rh_a. This interpretation is also related to the Bouchet's complementary hypothesis (Bouchet, 1963). Bouchet hypothesized that land surface wetness is coupled to the atmospheric state when there is negligible advection of humid air entering the system. In our PM_{rh} model, rh_s and rh_a are coevolving and consequently, they can be equal at daily time scale both "dry land-dry air" and "wet land-wet air" conditions (Fig. 3). This shows how land surface conditions become embedded in the near-surface atmospheric state.

As described in the theory section, land-atmosphere equilibrium is achieved when LE_G approaches zero and thus *LE* reduces to Eq. (6). The decomposed terms derived from both the empirical FLUXNET2015 and model-based FLUXCOM datasets show that the global mean for LE_G is near zero, implying global-scale land-atmosphere equilibrium (Fig. 4 and Fig. 5). This result extends the SFE theory of McColl et al. (2019). Although, LE_G is not always near zero (e.g., in low latitude regions where the influence of the ocean and atmospheric circulation on rh_a is significant (Byrne and O'Gorman, 2018)), moisture convergence and divergence at the global-scale tend to balance each other out, resulting in global-scale land-atmosphere equilibrium.

A number of important implications emerge from the global scale land-atmosphere equilibrium. (i) rh_a is a close approximation of rh_s at the global scale, and thus the decreasing trend of rh_a over the land surface predicted by climate models (Byrne and O'Gorman, 2016) and empirically observed (Willett et al., 2014) may indicate not only drier climatic conditions but also drier conditions for the land surface and soil moisture. (ii) Equation (6), which can be readily determined using standard meteorological measurements, can provide a fundamental benchmark of global scale *LE* which can be used to evaluate sophisticated land surface models.

6. Conclusions

We have shown that our novel PM_{rh} model provides a new opportunity to understand the governing physics of the terrestrial energy budget. Specifically, the PM_{rh} model helps to illustrate how the land surface conditions become encoded to the atmospheric state. "Dry land-dry air" or "wet land-wet air" conditions can each lead to daily scale land-atmosphere equilibrium. Our findings suggest that while LE_G is a primary component determining EF, spatiotemporal variability of LE_Q alone can adequately represent the variability of *LE*. We found global-scale land-atmosphere equilibrium at daily to annual scales, which

implies that *LE* can be simply determined by the atmospheric state and radiative energy without any surface constraint required to represent spatial heterogeneity and physiological influences. Therefore, our model can provide a fundamental benchmark against which *LE* predictions derived from climate models can be assessed. Questions remain regarding how LE_Q and LE_G will be influenced in relation to changing climatic and land surface conditions, and how these changes might affect the climate system at differing spatial and temporal scales through positive or negative feedbacks.

Appendix A

Derivation of Equation (2)

LE and *H* can be written using aerodynamic resistance for water vapour (r_{av}) and sensible heat (r_{aH}) as follows

$$LE = \frac{\rho c_p}{\gamma}\frac{rh_s e^*(T_s) - rh_a e^*(T_a)}{r_{av}} \quad \text{(A1)}$$

$$H = \rho c_p \frac{T_s - T_a}{r_{aH}} \quad \text{(A2)}$$

To express *LE* as a function of T_a and rh_s, adding $-rh_s e^*(T_a) + rh_s e^*(T_a)$ to the numerator of (A1) yields:

$$LE = \frac{\rho c_p}{\gamma}\frac{rh_s e^*(T_s) - rh_s e^*(T_a) + rh_s e^*(T_a) - rh_a e^*(T_a)}{r_{av}} = \frac{\rho c_p}{\gamma} rh_s \frac{e^*(T_s) - e^*(T_a)}{r_{av}} + \frac{\rho c_p}{\gamma} e^*(T_a)\frac{rh_s - rh_a}{r_{av}} \quad \text{(A3)}$$

Next, we use the linearized slope of e^* ($\frac{e^*(T_s) - e^*(T_a)}{T_s - T_a} \approx \frac{de^*}{dT}|_{T=T_a} = S$) to give

$$LE = \frac{\rho c_p}{\gamma} rh_s S \frac{T_s - T_a}{r_{av}} + \frac{\rho c_p}{\gamma} e^*(T_a)\frac{rh_s - rh_a}{r_{av}} \quad \text{(A4)}$$

If we assume $r_{aH} \approx r_{av} \approx r_a$, Eq. (A4) becomes

$$LE = rh_s \frac{S}{\gamma} H + \frac{\rho c_p}{\gamma} e^*(T_a)\frac{rh_s - rh_a}{r_a} \quad \text{(A5)}$$

Then, substituting the surface energy balance ($H = Q - LE$) into the first term of Eq. (A5):

$$LE = \underbrace{\frac{rh_s S}{rh_s S + \gamma} Q}_{Diabatic} + \underbrace{\frac{\rho c_p\, e^*(T_a)}{rh_s S + \gamma}\frac{rh_s - rh_a}{r_a}}_{Adiabatic} \quad \text{(A6)}$$

Derivation of Equation (3)

LE and *H* can be written using aerodynamic resistance for water vapour (r_{av}) and sensible heat (r_{aH}) as follows

$$LE = \frac{\rho c_p}{\gamma}\frac{rh_s e^*(T_s) - rh_a e^*(T_a)}{r_{av}} \quad \text{(A7)}$$

$$H = \rho c_p \frac{T_s - T_a}{r_{aH}} \quad \text{(A8)}$$

To express *LE* as a function of T_s and rh_a, adding $-rh_a e^*(T_s) + rh_a e^*(T_s)$ to the numerator of (A7) yields:

$$LE = \frac{\rho c_p}{\gamma}\frac{rh_s e^*(T_s) - rh_a e^*(T_s) + rh_a e^*(T_s) - rh_a e^*(T_a)}{r_{av}} = \frac{\rho c_p}{\gamma} e^*(T_s)\frac{rh_s - rh_a}{r_{av}} + \frac{\rho c_p}{\gamma} rh_a \frac{e^*(T_s) - e^*(T_a)}{r_{av}} \quad \text{(A9)}$$

Next, we use the linearized slope of e^* ($\frac{e^*(T_s) - e^*(T_a)}{T_s - T_a} \approx \frac{de^*}{dT}|_{T=T_a} = S$) to give

$$LE = \frac{\rho c_p}{\gamma} e^*(T_s)\frac{rh_s - rh_a}{r_{av}} + \frac{\rho c_p}{\gamma} rh_a S \frac{T_s - T_a}{r_{av}} \quad \text{(A10)}$$

If we assume $r_{aH} \approx r_{av} \approx r_a$, Eq. (A10) becomes

$$LE = \frac{\rho c_p}{\gamma} e^*(T_s)\frac{rh_s - rh_a}{r_a} + rh_a \frac{S}{\gamma} H \quad \text{(A11)}$$

Then, substituting the surface energy balance ($H = Q - LE$) into the second term of Eq. (A11):

$$LE = \underbrace{\frac{\rho c_p\, e^*(T_s)}{rh_a S + \gamma}\frac{rh_s - rh_a}{r_a}}_{Adiabatic} + \underbrace{\frac{rh_a S}{rh_a S + \gamma} Q}_{Diabatic} \quad \text{(A12)}$$

Data availability. The FLUXNET2015 dataset is available in https://fluxnet.org/data/fluxnet2015-dataset/. The highlighted sugarcane eddy covariance site dataset will be available in AmeriFlux (https://ameriflux.lbl.gov/). The FLUXCOM dataset is available in http://www.fluxcom.org/.

Author contribution. Y.K. and M.S.J. designed research; U.W. provided FLUXCOM data; Y.K., L.M., and M.S.J. performed research; Y.K. analyzed data; Y.K., M.G., T.A.B, L.M., and M.S.J. wrote the paper.

Competing interests. The authors declare no conflict of interest.

Acknowledgements. We want to thank Dr. Iain Hawthorne, Pável Bautista, Dr. Silja Hund, Cameron Webster, Gretel Rojas Hernandez, Guillermo Duran Sanabria, Dr. Andrea Suarez Serrano, Dr. Ana Maria Duran, Martin Martinez, and Dr. Fermín Subirós Ruiz for field and logistical support. We also thank Dr. Martin Jung, the principal investigator of the FLUXCOM dataset. The authors would like to thank the EU and NSERC for funding, in the frame of the collaborative international Consortium AgWIT financed under the ERA-NET WaterWorks2015 Cofunded Call. This ERA-NET is an integral part of the 2016 Joint Activities developed by the Water Challenges for a Changing World Joint Programme Initiative (Water JPI).

References

Baldocchi, D., Falge, E., Gu, L., Olson, R., Hollinger, D., Running, S., Anthoni, P., Bernhofer, C., Davis, K., and Evans, R.: FLUXNET: A new tool to study the temporal and spatial variability of ecosystem-scale carbon dioxide, water vapor, and energy flux densities, Bulletin of the American Meteorological Society, 82, 2415-2434, 10.1175/1520-0477(2001)082<2415:FANTTS>2.3.CO;2 2001.

Bouchet, R. J.: Evapotranspiration réelle et potentielle, signification climatique, IAHS Publ, 62, 134-142, 1963.

Byrne, M. P., and O'Gorman, P. A.: Understanding Decreases in Land Relative Humidity with Global Warming: Conceptual Model and GCM Simulations, Journal of Climate, 29, 9045-9061, 10.1175/jcli-d-16-0351.1, 2016.

Byrne, M. P., and O'Gorman, P. A.: Trends in continental temperature and humidity directly linked to ocean warming, Proceedings of the National Academy of Sciences, 115, 4863-4868, 10.1073/pnas.1722312115, 2018.

Eichinger, W. E., Parlange, M. B., and Stricker, H.: On the Concept of Equilibrium Evaporation and the Value of the Priestley-Taylor Coefficient, Water Resources Research, 32, 161-164, 10.1029/95wr02920, 1996.

Eshonkulov, R., Poyda, A., Ingwersen, J., Pulatov, A., and Streck, T.: Improving the energy balance closure over a winter wheat field by accounting for minor storage terms, Agricultural and Forest Meteorology, 264, 283-296, 10.1016/j.agrformet.2018.10.012, 2019.

Fisher, J. B., Tu, K. P., and Baldocchi, D. D.: Global estimates of the land–atmosphere water flux based on monthly AVHRR and ISLSCP-II data, validated at 16 FLUXNET sites, Remote Sensing of Environment, 112, 901-919, 10.1016/j.rse.2007.06.025, 2008.

Foken, T.: The energy balance closure problem: an overview, Ecological Applications, 18, 1351-1367, 10.1890/06-0922.1, 2008.

García, M., Sandholt, I., Ceccato, P., Ridler, M., Mougin, E., Kergoat, L., Morillas, L., Timouk, F., Fensholt, R., and Domingo, F.: Actual evapotranspiration in drylands derived from in-situ and satellite data: Assessing biophysical constraints, Remote Sensing of Environment, 131, 103-118, 10.1016/j.rse.2012.12.016, 2013.

Gentine, P., Entekhabi, D., Chehbouni, A., Boulet, G., and Duchemin, B.: Analysis of evaporative fraction diurnal behaviour, Agricultural and Forest Meteorology, 143, 13-29, 10.1016/j.agrformet.2006.11.002, 2007.

Gentine, P., Entekhabi, D., and Polcher, J.: The Diurnal Behavior of Evaporative Fraction in the Soil–Vegetation–Atmospheric Boundary Layer Continuum, Journal of Hydrometeorology, 12, 1530-1546, 10.1175/2011jhm1261.1, 2011.

Hatala, J. A., Detto, M., and Baldocchi, D. D.: Gross ecosystem photosynthesis causes a diurnal pattern in methane emission from rice, Geophysical Research Letters, 39, 1-5, 10.1029/2012GL051303, 2012.

Hersbach, H., Bell, B., Berrisford, P., Hirahara, S., Horányi, A., Muñoz-Sabater, J., Nicolas, J., Peubey, C., Radu, R., and Schepers, D.: The ERA5 global reanalysis, Quarterly Journal of the Royal Meteorological Society, 146, 1999-2049, 2020.

Hund, S. V., Allen, D. M., Morillas, L., and Johnson, M. S.: Groundwater recharge indicator as tool for decision makers to increase socio-hydrological resilience to seasonal drought, Journal of Hydrology, 563, 1119-1134, 10.1016/j.jhydrol.2018.05.069, 2018.

Iribarne, J. V., and Godson, W. L.: Atmospheric thermodynamics, Springer Science & Business Media, 2012.

Jarvis, P. G., and McNaughton, K. G.: Stomatal control of transpiration: scaling up from leaf to region, in: Advances in ecological research, Elsevier, 1-49, 1986.

Johnson, M. S., Couto, E. G., Pinto Jr, O. B., Milesi, J., Santos Amorim, R. S., Messias, I. A. M., and Biudes, M. S.: Soil CO2 Dynamics in a Tree Island Soil of the Pantanal: The Role of Soil Water Potential, PLOS ONE, 8, e64874, 10.1371/journal.pone.0064874, 2013.

Jung, M., Koirala, S., Weber, U., Ichii, K., Gans, F., Camps-Valls, G., Papale, D., Schwalm, C., Tramontana, G., and Reichstein, M.: The FLUXCOM ensemble of global land-atmosphere energy fluxes, Scientific Data, 6, 74, 10.1038/s41597-019-0076-8, 2019.

Kleidon, A., and Schymanski, S.: Thermodynamics and optimality of the water budget on land: A review, Geophysical Research Letters, 35, 10.1029/2008gl035393, 2008.

Kleidon, A., Schymanski, S., and Stieglitz, M.: Thermodynamics, Irreversibility, and Optimality in Land Surface Hydrology, in: Bioclimatology and Natural Hazards, edited by: Střelcová, K., Mátyás, C., Kleidon, A., Lapin, M., Matejka, F., Blaženec, M., Škvarenina, J., and Holécy, J., Springer Netherlands, Dordrecht, 107-118, 2009.

Knauer, J., El-Madany, T. S., Zaehle, S., and Migliavacca, M.: Bigleaf—An R package for the calculation of physical and physiological ecosystem properties from eddy covariance data, PLOS ONE, 13, e0201114, 10.1371/journal.pone.0201114, 2018.

Leuning, R., van Gorsel, E., Massman, W. J., and Isaac, P. R.: Reflections on the surface energy imbalance problem, Agricultural and Forest Meteorology, 156, 65-74, 10.1016/j.agrformet.2011.12.002, 2012.

Lovell-Smith, J. W., Feistel, R., Harvey, A. H., Hellmuth, O., Bell, S. A., Heinonen, M., and Cooper, J. R.: Metrological challenges for measurements of key climatological observables. Part 4: atmospheric relative humidity, Metrologia, 53, R40-R59, 10.1088/0026-1394/53/1/r40, 2015.

Ma, H.-Y., Klein, S. A., Xie, S., Zhang, C., Tang, S., Tang, Q., Morcrette, C. J., Van Weverberg, K., Petch, J., Ahlgrimm, M., Berg, L. K., Cheruy, F., Cole, J., Forbes, R., Gustafson Jr, W. I., Huang, M., Liu, Y., Merryfield, W., Qian, Y., Roehrig, R., and Wang, Y.-C.: CAUSES: On the Role of Surface Energy Budget Errors to the Warm Surface Air Temperature Error Over the Central United States, Journal of Geophysical Research: Atmospheres, 123, 2888-2909, 10.1002/2017jd027194, 2018.

Mallick, K., Jarvis, A. J., Boegh, E., Fisher, J. B., Drewry, D. T., Tu, K. P., Hook, S. J., Hulley, G., Ardö, J., Beringer, J., Arain, A., and Niyogi, D.: A Surface Temperature Initiated Closure (STIC) for surface energy balance fluxes, Remote Sensing of Environment, 141, 243-261, 10.1016/j.rse.2013.10.022, 2014.

Martens, B., Miralles, D. G., Lievens, H., van der Schalie, R., de Jeu, R. A. M., Fernandez-Prieto, D., Beck, H. E., Dorigo, W. A., and Verhoest, N. E. C.: GLEAM v3: satellite-based land evaporation and root-zone soil moisture, Geoscientific Model Development, 10, 1903-1925, 10.5194/gmd-10-1903-2017, 2017.

Massmann, A., Gentine, P., and Lin, C.: When Does Vapor Pressure Deficit Drive or Reduce Evapotranspiration?, Journal of Advances in Modeling Earth Systems, 11, 3305-3320, 10.1029/2019ms001790, 2019.

McColl, K. A., Salvucci, G. D., and Gentine, P.: Surface Flux Equilibrium Theory Explains an Empirical Estimate of Water-Limited Daily Evapotranspiration, Journal of Advances in Modeling Earth Systems, 11, 2036-2049, 10.1029/2019ms001685, 2019.

McColl, K. A.: Practical and Theoretical Benefits of an Alternative to the Penman-Monteith Evapotranspiration Equation, Water Resources Research, 56, e2020WR027106, 10.1029/2020wr027106, 2020.

McColl, K. A., and Rigden, A. J.: Emergent simplicity of continental evapotranspiration, Geophysical Research Letters, n/a, e2020GL087101, 10.1029/2020gl087101, 2020.

McNaughton, K., and Spriggs, T.: An evaluation of the Priestley and Taylor equation and the complementary relationship using results from a mixed-layer model of the convective boundary layer, IAHS publication, 177, 89-104, 1989.

McNaughton, K. G., and Jarvis, P. G.: Predicting effects of vegetation changes on transpiration and evaporation, Water deficits and plant growth, 7, 1-47, 1983.

Monteith, J., and Unsworth, M.: Principles of environmental physics: plants, animals, and the atmosphere, Academic Press, 2013.

Monteith, J. L.: Evaporation and environment, Symposia of the society for experimental biology, 1965, 205-234,

Monteith, J. L.: Evaporation and surface temperature, Quarterly Journal of the Royal Meteorological Society, 107, 1-27, 10.1002/qj.49710745102, 1981.

Moon, M., Li, D., Liao, W., Rigden, A. J., and Friedl, M. A.: Modification of surface energy balance during springtime: The relative importance of biophysical and meteorological changes, Agricultural and Forest Meteorology, 284, 107905, 10.1016/j.agrformet.2020.107905, 2020.

Morillas, L., Hund, S. V., and Johnson, M. S.: Water Use Dynamics in Double Cropping of Rainfed Upland Rice and Irrigated Melons Produced Under Drought-Prone Tropical Conditions, Water Resources Research, 0, 10.1029/2018wr023757, 2019.

Novick, K. A., Ficklin, D. L., Stoy, P. C., Williams, C. A., Bohrer, G., Oishi, A. C., Papuga, S. A., Blanken, P. D., Noormets, A., Sulman, B. N., Scott, R. L., Wang, L., and Phillips, R. P.: The increasing importance of atmospheric demand for ecosystem water and carbon fluxes, Nat Clim Change, 6, 1023, 10.1038/nclimate3114, 2016.

Oki, T., and Kanae, S.: Global hydrological cycles and world water resources, Science, 313, 1068-1072, 2006.

Pastorello, G., Trotta, C., Canfora, E., Chu, H., Christianson, D., Cheah, Y.-W., Poindexter, C., Chen, J., Elbashandy, A., Humphrey, M., Isaac, P., Polidori, D., Ribeca, A., van Ingen, C., Zhang, L., Amiro, B., Ammann, C., Arain, M. A., Ardö, J., Arkebauer, T., Arndt, S. K., Arriga, N., Aubinet, M., Aurela, M., Baldocchi, D., Barr, A., Beamesderfer, E., Marchesini, L. B., Bergeron, O., Beringer, J., Bernhofer, C., Berveiller, D., Billesbach, D., Black, T. A., Blanken, P. D., Bohrer, G., Boike, J., Bolstad, P. V., Bonal, D., Bonnefond, J.-M., Bowling, D. R., Bracho, R., Brodeur, J., Brümmer, C., Buchmann, N., Burban, B., Burns, S. P., Buysse, P., Cale, P., Cavagna, M., Cellier, P., Chen, S., Chini, I., Christensen, T. R., Cleverly, J., Collalti, A., Consalvo, C., Cook, B. D., Cook, D., Coursolle, C., Cremonese, E., Curtis, P. S., D'Andrea, E., da Rocha, H., Dai, X., Davis, K. J., De Cinti, B., de Grandcourt, A., De Ligne, A., De Oliveira, R. C., Delpierre, N., Desai, A. R., Di Bella, C. M., di Tommasi, P., Dolman, H., Domingo, F., Dong, G., Dore, S., Duce, P., Dufrêne, E., Dunn, A., Dušek, J., Eamus, D., Eichelmann, U., ElKhidir, H. A. M., Eugster, W., Ewenz, C. M., Ewers, B., Famulari, D., Fares, S., Feigenwinter, I., Feitz, A., Fensholt, R., Filippa, G., Fischer, M., Frank, J., Galvagno, M., Gharun, M., Gianelle, D., Gielen, B., Gioli, B., Gitelson, A., Goded, I., Goeckede, M., Goldstein, A. H., Gough, C. M., Goulden, M. L., Graf, A., Griebel, A., Gruening, C., Grünwald, T., Hammerle, A., Han, S., Han, X., Hansen, B. U., Hanson, C., Hatakka, J., He, Y., Hehn, M., Heinesch, B., Hinko-Najera, N., Hörtnagl, L., Hutley, L., Ibrom, A., Ikawa, H., Jackowicz-Korczynski, M., Janouš, D., Jans, W., Jassal, R., Jiang, S., Kato, T., Khomik, M., Klatt, J., Knohl, A., Knox, S., Kobayashi, H., Koerber, G., Kolle, O., Kosugi, Y., Kotani, A., Kowalski, A., Kruijt, B., Kurbatova, J., Kutsch, W. L., Kwon, H., Launiainen, S., Laurila, T., Law, B., Leuning, R., Li, Y., Liddell, M., Limousin, J.-M., Lion, M., Liska, A. J., Lohila, A., López-Ballesteros, A., López-Blanco, E., Loubet, B., Loustau, D., Lucas-Moffat, A., Lüers, J., Ma, S., Macfarlane, C., Magliulo, V., Maier, R., Mammarella, I., Manca, G., Marcolla, B., Margolis, H. A., Marras, S., Massman, W., Mastepanov, M., Matamala, R., Matthes, J. H., Mazzenga, F., McCaughey, H., McHugh, I., McMillan, A. M. S., Merbold, L., Meyer, W., Meyers, T., Miller, S. D., Minerbi, S., Moderow, U., Monson, R. K., Montagnani, L., Moore, C. E., Moors, E., Moreaux, V., Moureaux, C., Munger, J. W., Nakai, T., Neirynck, J., Nesic, Z., Nicolini, G., Noormets, A., Northwood, M., Nosetto, M., Nouvellon, Y., Novick, K., Oechel, W., Olesen, J. E., Ourcival, J.-M., Papuga, S. A., Parmentier, F.-J., Paul-Limoges, E., Pavelka, M., Peichl, M., Pendall, E., Phillips, R. P., Pilegaard, K., Pirk, N., Posse, G., Powell, T., Prasse, H., Prober, S. M., Rambal, S., Rannik, Ü., Raz-Yaseef, N., Reed, D., de Dios, V. R., Restrepo-Coupe, N., Reverter, B. R., Roland, M., Sabbatini, S., Sachs, T., Saleska, S. R., Sánchez-Cañete, E. P., Sanchez-Mejia, Z. M., Schmid, H. P., Schmidt, M., Schneider, K., Schrader, F., Schroder, I., Scott, R. L., Sedlák, P., Serrano-Ortíz, P., Shao, C., Shi, P., Shironya, I., Siebicke, L., Šigut, L., Silberstein, R., Sirca, C., Spano, D., Steinbrecher, R., Stevens, R. M., Sturtevant, C., Suyker, A., Tagesson, T., Takanashi, S., Tang, Y., Tapper, N., Thom, J., Tiedemann, F., Tomassucci, M., Tuovinen, J.-P., Urbanski, S., Valentini, R., van der Molen, M., van Gorsel, E., van Huissteden, K., Varlagin, A., Verfaillie, J., Vesala, T., Vincke, C., Vitale, D., Vygodskaya, N., Walker, J. P., Walter-Shea, E., Wang, H., Weber, R., Westermann, S., Wille, C., Wofsy, S., Wohlfahrt, G., Wolf, S., Woodgate, W., Li, Y., Zampedri, R., Zhang, J., Zhou, G., Zona, D., Agarwal, D., Biraud, S., Torn, M., and Papale, D.: The FLUXNET2015 dataset and the ONEFlux processing pipeline for eddy covariance data, Scientific Data, 7, 225, 10.1038/s41597-020-0534-3, 2020.

Penman, H. L.: Natural evaporation from open water, bare soil and grass, Proceedings of the Royal Society of London. Series A. Mathematical and Physical Sciences, 193, 120-145, 1948.

Priestley, C. H. B., and Taylor, R. J.: On the Assessment of Surface Heat Flux and Evaporation Using Large-Scale Parameters, Monthly Weather Review, 100, 81-92, 10.1175/1520-0493(1972)100<0081:otaosh>2.3.co;2, 1972.

Ramírez, J. A., Hobbins, M. T., and Brown, T. C.: Observational evidence of the complementary relationship in regional evaporation lends strong support for Bouchet's hypothesis, Geophysical Research Letters, 32, 10.1029/2005gl023549, 2005.

Raupach, M. R.: Combination theory and equilibrium evaporation, Quarterly Journal of the Royal Meteorological Society, 127, 1149-1181, 10.1002/qj.49712757402, 2001.

Rigden, A. J., and Salvucci, G. D.: Evapotranspiration based on equilibrated relative humidity (ETRHEQ): Evaluation over the continental U.S, Water Resources Research, 51, 2951-2973, 10.1002/2014wr016072, 2015.

Rigden, A. J., and Salvucci, G. D.: Stomatal response to humidity and CO2 implicated in recent decline in US evaporation, Global Change Biology, 23, 1140-1151, 10.1111/gcb.13439, 2017.

Roesch, A., and Schmidbauer, H.: WaveletComp: Computational Wavelet Analysis, 2014.

Salvucci, G. D., and Gentine, P.: Emergent relation between surface vapor conductance and relative humidity profiles yields evaporation rates from weather data, Proceedings of the National Academy of Sciences, 110, 6287-6291, 10.1073/pnas.1215844110, 2013.

Sherwood, S., and Fu, Q.: A Drier Future?, Science, 343, 737-739, 10.1126/science.1247620, 2014.

Stoy, P. C., Mauder, M., Foken, T., Marcolla, B., Boegh, E., Ibrom, A., Arain, M. A., Arneth, A., Aurela, M., Bernhofer, C., Cescatti, A., Dellwik, E., Duce, P., Gianelle, D., van Gorsel, E., Kiely, G., Knohl, A., Margolis, H., McCaughey, H., Merbold, L., Montagnani, L., Papale, D., Reichstein, M., Saunders, M., Serrano-Ortiz, P., Sottocornola, M., Spano, D., Vaccari, F., and Varlagin, A.: A data-

driven analysis of energy balance closure across FLUXNET research sites: The role of landscape scale heterogeneity, Agricultural and Forest Meteorology, 171-172, 137-152, 10.1016/j.agrformet.2012.11.004, 2013.

Tan, C. S., Black, T. A., and Nnyamah, J. U.: A Simple Diffusion Model of Transpiration Applied to a Thinned Douglas-Fir Stand, Ecology, 59, 1221-1229, 10.2307/1938235, 1978.

Thom, A. S.: Momentum, mass and heat exchange of vegetation, Quarterly Journal of the Royal Meteorological Society, 98, 124-134, 10.1002/qj.49709841510, 1972.

Willett, K., Dunn, R., Thorne, P., Bell, S., De Podesta, M., Parker, D., Jones, P., and Williams Jr, C.: HadISDH land surface multi-variable humidity and temperature record for climate monitoring, Climate of the Past, 10, 2014.

Wilson, K., Goldstein, A., Falge, E., Aubinet, M., Baldocchi, D., Berbigier, P., Bernhofer, C., Ceulemans, R., Dolman, H., Field, C., Grelle, A., Ibrom, A., Law, B. E., Kowalski, A., Meyers, T., Moncrieff, J., Monson, R., Oechel, W., Tenhunen, J., Valentini, R., and Verma, S.: Energy balance closure at FLUXNET sites, Agricultural and Forest Meteorology, 113, 223-243, 10.1016/S0168-1923(02)00109-0, 2002.